Binding of Rigid Dendritic Ruthenium Complexes to Carbon Nanotubes

H. Chaturvedi and J. C. Poler*

Department of Chemistry and Center for Optoelectronics and Optical Communications, University of North Carolina at Charlotte, 9201 University City Boulevard, Charlotte, North Carolina 28223

Received: March 29, 2006; In Final Form: July 15, 2006

Single-walled carbon nanotubes (SWNTs) bind strongly to rigid ruthenium metallodendrimers. High valence ions effectively coagulate these nanotubes from stable dispersions in *N*,*N*-dimethylforamide. While ruthenium salts and small $[Ru(diimine)_3]^{2+}$ complexes also coagulate the nanotubes, they require much higher concentrations and are easily extracted from the nanotubes with acetonitrile. Enantiomerically pure ruthenium metallodendrimer $[\Lambda_6\Delta_3\Lambda\text{-}Ru_{10}]^{20+}[PF_6^-]_{20}$ is shown to bind strongly and specifically to the SWNTs. Most of the nanotube's ends are functionalized with this large (5.8 nm), optically active, rigid supramolecular complex. We study the binding capacity with UV−vis and atomic absorption spectroscopy. Imaging the functionalized nanotubes with scanning electron microscopy and atomic force microscopy (AFM) yields direct confirmation of end functionalization. Statistical analysis of the AFM images shows the morphology of the functionalized ends is consistent with the nanotubes binding to one of the endo- or exoreceptors around the dendrimer. Implications of these results toward efficient nanomanufacturing of carbon nanotube devices are discussed.

I. Introduction

Carbon nanotubes (CNTs) have made a significant technological impact in the fields of nanotechnology,[1] nanoelectronics,[2−4] and optoelectronics.[5] To advance further the myriad of applications that use CNTs, there must be a significant improvement in the purity, polydispersity, and assembly of the tubes. These advances will allow far greater fidelity in constructing advanced electronic, optical, and mechanical devices of nanometer scale and reduced dimensionality. Our long-term goal, related to the results described below, is to develop efficient manufacturing schemes for nanostructured materials constructed of and connected by CNTs.

There have been significant advances in the purity and functionalization of single-walled carbon nanotubes (SWNTs) using various ionic,[6,7] molecular,[8] polymer,[9] nucleic acid,[10,11] and nanoparticle[12] adsorption and binding strategies. CNTs can be functionalized through physisorption[13,14] and covalent[15,16] attachment. Covalent attachment of multiwalled carbon nanotubes through ruthenium diimine linkage shows the potential of CNT assembly.[17] Our aim is to functionalize CNTs with large rigid molecular systems that can mechanically[18,19] dock to, or about, the nanoparticle. The advantage of this approach is that it may be possible to connect nanotubes and nanowires together into topologically stable and morphologically static three-dimensional (3D) assemblies.

To attach and assemble SWNTs together, we require molecular systems that are similar in size to the diameter of the nanotube. The diameter of a CNT is calculated from $(n^2 + m^2 + nm)^{0.5}\cdot 0.783$ Å, where the vector (n,m) describes its chirality.[20] As-purchased SWNTs are polydisperse with a typical range of diameters from 0.7 to 2.1 nm. Whereas many polymer particles, polynucleic acids, and proteins have these dimensions in solution, they are too flexible to maintain a rigid assembly. We are using a class of supramolecular dendritic complexes[21] that have the desired properties for our 3D nanoassembly process. The supramolecular system we describe below was first synthesized by F. M. MacDonnell[22−24] at the University of Texas at Arlington.

Supramolecular systems are composed of bound molecular units that extend over several nanometers, significantly larger than most covalently bound molecules.[25] Dendritic supramolecules are often grown by covalently attaching the next generation of molecular units through bonds which have significant free rotation and therefore nonrigid morphology. Dendrimers can also employ mechanical interlocking to build extensive chemical systems.[26] Moreover, while many dendrimers are topologically well described, their equilibrium geometry is typically globular and does not enable spatially directed attachment or assembly to nanoparticles.

Supramolecular dendrimers synthesized from enantiomerically pure $[Ru(diimine)_3]^{2+}$ units have allowed MacDonnell to build large multimetal rigid metallodendrimers.[27] Specifically, we are using the $[\Lambda_6\Delta_3\Lambda\text{-}Ru_{10}]^{20+}[PF_6^-]_{20}$ metallodendrimer. This decamer was formed by reacting three Δ-$[Ru(diimine)_3]^{2+}$ units to the central Λ-$[Ru(diimine)_3]^{2+}$ unit and finally six Λ-$[Ru(diimine)_3]^{2+}$ units to form the large supramolecular system shown in Figure 1. Previously reported semiempirical (PM3) computation and spectroscopic characterization of this decamer[21] confirm that the molecule is planar, highly symmetric, and rigid with respect to molecular fluctuation. While all of the Ru centers lie in a plane, the complex is 3D with a thickness of 0.9 nm. Figure 1 illustrates the decamer mechanically docked around an A(10,10) CNT [$d = 1.36$ nm] (geometry optimized by UFF molecular mechanics). Close contact van der Waals (vdW) interactions between the tube and the cavity of the decamer are indicated. While it is not clear how this molecule does bind to CNTs, our results below indicate a strong interaction. We refer to three types of potential binding sites to the decamer. The electron density of the delocalized electrons on the aromatic

* To whom correspondence should be addressed. E-mail: jcpoler@email.uncc.edu. Tel: 704 687-3064. Fax: 704 687-3151.

10.1021/jp061952f CCC: $33.50
Published on Web 10/24/2006

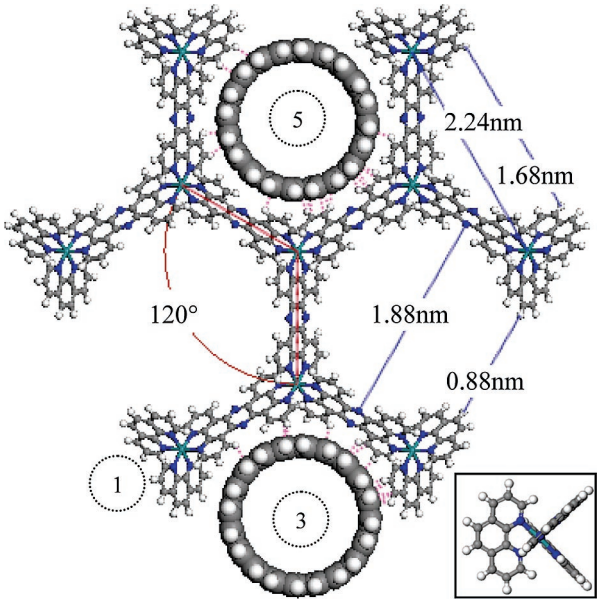

Figure 1. PM3 Geometry optimized ruthenium decamer illustrated with DFT Geometry optimized SWNT A(10,10) (CPK model) interacting through clefts and pockets about the decamer. Binding sites are enumerated by the number of nearest neighbor metal centers to the CNT. Preliminary AM1 semiempirical calculations indicate a binding energy of −120 kcal/mol for a CNT interacting within a supramolecular pocket similar to binding site "5" above. The outer vdW diameter of an A(10,10) CNT is 1.70 nm. Distances indicated on the decamer are measured between the indicated atoms, reduced by the atom's vdW radii. Third generation ruthenium nuclei of the "three-centered" cleft are separated by 2.24 nm. Close contacts are illustrated by dashed lines. The largest distance across the decamer is 5.85 nm. The distance from the bottom of the bound CNT in site "3" to the top of the decamer is calculated to be 5.88 nm. The inset shows a model of the "monomer" unit $Ru(phen)_3$ looking down the edge of exoreceptor site "1".

phenanthroline ligands should physisorb to the surface of the CNTs through $\pi-\pi$ stacking interactions.[28] Along the circumference of the decamer are six clefts formed between the outer two phenanthroline ligands of these $[Ru(tpphz)(phenanthroline)_2]^{2+}$ units (tpphz = phenazine bridging ligand between two Ru centers). Small diameter CNTs can fit well into this "one-centered" exoreceptor (labeled "1" in Figure 1). Larger nanotubes can fit onto a "three-centered" exoreceptor (labeled "3" in Figure 1). The surface of this cleft is composed of two tetrapyrido-phenazine bridging ligands connecting one of the second-generation Ru centers to two of the third-generation Ru centers. A phenathroline ligand on each of these outermost Ru centers enlarges the cleft to wrap almost 180° around a CNT. A "five-centered" pocket or endoreceptor is indicated in Figure 1 (labeled "5") by the placement of an A(10,10) CNT bound within. Additionally, the decamer can also lie flat along the nanotube. These binding motifs will be discussed below in relation to our spectroscopic and atomic force microscopy (AFM) data.

II. Experimental Section

All SWNTs were used as purchased (Carbon Nanotechnologies Inc. Grade P). Stable dispersions of the CNTs were made in wet *N*,*N*-dimethylforamide (DMF) (Aldrich, as-received). From Karl-Fisher coulometric titration (Mettler Toledo DL32), the DMF contained 3500 ppm of water. Dispersions were made by adding excess (~1.0 mg) CNT powder into 100 mL of DMF and ultrasonicated for 30 min at 10 W (RMS) power (Fisher Model 60 1/8" probe tip). The solution's temperature increases during sonication. The opaque black solution is filtered through glass wool to yield a clear and gray CNT solution. CNT solution concentrations of 7 mg/L were estimated from UV−Vis spectroscopy (Cary 300) by measuring the optical density[29] at 500 nm. These dispersions were stable for weeks to months.

All ruthenium reagents were used as available. Stock solutions of $[\Lambda_6\Delta_3\Lambda\text{-}Ru_{10}]^{20+}[PF_6^-]_{20}$ (gift from F. M. MacDonnell) and of $[Ru(phenthroline)_3]^{2+}[PF_6^-]_2$ were prepared in dry acetonitrile (MeCN). Using MacDonnell's notation, we refer to the $[\Lambda_6\Delta_3\Lambda\text{-}Ru_{10}]^{20+}[PF_6^-]_{20}$ compound as the decamer since it is composed from 10 units of modified $[Ru(phenthroline)_3]^{2+}[PF_6^-]_2$ which we refer to as the monomer. Stock solutions of $RuCl_3$ in wet DMF were prepared from 1000 ppm $RuCl_{3(aq)}$ in 10% $HCl_{(aq)}$ (Perkin-Elmer Atomic Spectroscopy Standard).

Ruthenium complexes are highly absorbing in the UV−Vis spectrum and easily monitored. Concentrations of the ruthenium complexes in dispersions were measured by calibration against known standards. Decamer concentrations of 5×10^{-8} M (5 ppb Ru) are above the sensitivity limit of our spectrometer.

To estimate the amount of ruthenium complex bound to the CNTs, we used atomic absorption (AA) spectroscopy (Perkin Elmer AA200). We injected 10−20 μL of dispersion into a graphite furnace (PE HGA900) and atomized the sample at 2500 °C. All AA measurements were calibrated against standard solutions of $RuCl_{3(aq)}$ in 10% HCL diluted into DMF. Due to systematic errors, our detection limit for Ru was 2 ppb (2×10^{-8} M decamer in solution).

Microscopic analysis of deposited nanotubes was acquired from field emission scanning electron microscopy (FE-SEM) (Raith150 with a Leo Gemini column). SEM images were acquired at 10 kV or lower. Energy-dispersive X-ray spectroscopy (EDX) was acquired using an EDAX Genesis 2000 on a JEOL JSM 4640LV SEM. Atomic force microscopy (AFM) images were acquired from two different AFMs (Digital Instruments Dimension 3100 with a Nanoscope IV controller and a Burleigh Metris 2000NC) and numerous probes to ensure consistency and preclude scanning artifacts that are systematic to this technique. AFM images were acquired in contact mode with the probe force optimized to reduce nanotube displacement from the scanning tip. AFM images were stable upon multiple scanning taken in different scan directions. Bright spots at the ends of the CNTs are associated with the decamer coagulation. These bright spots are never found in control experiments on pristine deposited CNTs. For control experiments, salts of $RuCl_3$ or $[Ru(phenanthroline)_3][PF_6]_2$, the bright spots are not associated/bound to the CNT ends after coagulation. While bright spots in AFM images are found on the surface after deposition of coagulated tubes, they are easily washed away with acetonitrile (MeCN). They are not present in the AFM images if the flocs are first extracted with MeCN before deposition of the tubes. Bright spots which we refer to as "particles" are concluded to be decamer bound to CNT ends as described below. The bound decamer is stable and not washed from the tubes with MeCN extractions either prior to deposition or washing after deposition.

CNTs were deposited onto oxide-coated silicon wafers by either drop casting or molecular combing.[30] The results shown below are all from drop casting 10 μL of dispersion on the substrate at room temperature. Samples were dried in flowing air in a laminar flow hood (<100 particles/m^3) for ~12 h. DMF drops evaporate quickly but leave residual DMF which dissipates in several hours. Control experiments on pure DMF resulted in clean flat substrates as observed by AFM. Drop casting results in inhomogeneous distributions of CNTs across the wafer. Nanotube alignment from drop casting is a result of the solvent

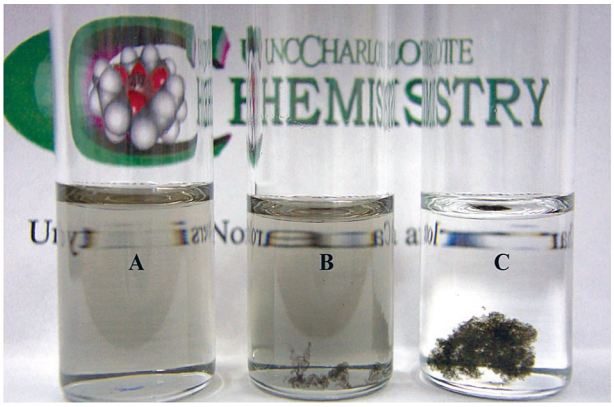

Figure 2. Image of CNTs dispersed in DMF at 7 mg/L two weeks after the addition of various ruthenium complexes: (A) 10^{-7} M monomer, (B) 10^{-9} M decamer, and (C) 10^{-7} M decamer.

evaporating and pulling the tubes through the solid−liquid−vapor contact line. As the DMF evaporates, and the concentration of the CNTs and ruthenium complexes increases, so does the density of particles deposited on the surface. Individual nanotubes are found hundreds of micrometers from where the "bulk" of the dispersed material deposits. Each sample was scanned at many locations and representative images are presented below. All lateral dimensions from AFM are convoluted with the radii of curvature of the AFM probe tip (~25 nm). We made no attempt to deconvolute the tip from the image. AFM images are flattened (1st order) to remove scanning artifacts and plane-fit to remove sample tilt. The contrast and brightness of images were manipulated to optimize clarity.

Extraction experiments were performed to discern precipitation of residual ruthenium complex, from ruthenium complex that is more strongly bound to the nanotubes. After the CNTs coagulate, the flocs are separated from solution by centrifugation at 7000 g. The supernatant is decanted, and the flocs are redispersed in MeCN, an excellent solvent for all of the ruthenium salts and complexes in this paper. Coagulated CNTs are then collected by centrifugation, decanting of the ruthenium containing supernatant, and then redispersed into DMF for deposition.

III. Results and Discussion

As-purified CNTs can be dispersed into many organic solvents at low, but useful, concentrations.[29] These solutions are kinetically stable for weeks to years depending on their degree of oxidation, purity, and length.[31] It is well understood that increasing the ionic strength of CNT dispersions will destabilize the solution[32] and result in the coagulation of colloidal nanotubes into a floc.[33] As expected, addition of ruthenium complex salts at sufficient concentration also coagulates the CNT dispersions. Coagulation of CNTs dispersed in aqueous electrolyte has been well described by Sano.[32] Under their conditions, the critical coagulation concentration (ccc) of $Z = 2+$ cations is in the 200 μM range and they found that the Schulze−Hardy rule[33−35] is followed for electrolytes of $Z = 1+$, $2+$, and $3+$ cations interacting with SWNTs. The image in Figure 2 demonstrates the effect of adding ruthenium salts to stable CNT dispersions. All three solutions were made from 7 mg/L SWNT in DMF. After brief sonication, a small amount of ruthenium complex was added. Addition of monomer to 10^{-7} M does not result in any coagulation, and the solution of Figure 2A was stable for weeks. Flocculation with the monomer starts to occur at ~10^{-6} M. These dispersions become unstable when the electric potential between the nanotubes goes to zero, for tubes separated by less than the Debye length. Increasing the ionic strength of the solution decreases the Debye length and results in nanotube coagulation. We observe this for the addition of ruthenium monomer, $RuCl_3$, and ruthenium decamer. Flocculation starts to occur at 10^{-9} M concentrations of ruthenium decamer as indicated by the small flocs near the bottom of the solution in Figure 2B. Figure 2C is of a solution that has completely collapsed into a large low-density floc less than an hour after the addition of ruthenium decamer at 10^{-7} M. The valence of our cation is extraordinarily large $Z = 20+$. According to the Schulze−Hardy rule, the ccc scales with the valency of the charged coagulant, ccc $\sim Z^{-6}$. The ruthenium decamer which we are studying is an asymmetric ionic compound. For asymmetric ionic compounds such as ours, we have reformulated the Schulze−Hardy rule and find that the ccc should scale as ccc $\sim (Z^2 + Z)^{-3}$, which is similar to the Schulze−Hardy rule. Accordingly, if our $Z = 2+$ ruthenium monomer coagulates the CNT solution at 10^{-6} M, then the $Z = 20+$ ruthenium decamer should collapse the dispersion at a concentration as low as 3×10^{-12} M. This high valence cation is not as effective as predicted indicating that, in addition to being a charged flocculant, there may be other interactions. Because of the decamer's large size (5.5 nm across), distributing the charge over an area several times larger than its molecular thickness, the decamer may need to be treated as a surface charge. Moreover, it is understood that high valence ions can bind strongly to surfaces in solution.[35,36] We believe the decamer is binding to the nanotubes in an interesting way. From UV−Vis and AA spectroscopy, there is no detectable Ru in the solution away from the floc in Figure 2C. Additionally, AA of 10 μL aliquots from the floc removed from the solution of Figure 2C is consistent with the total amount of Ru added to the CNT solution. Conversly, the solution away from the flocs formed from a monomer coagulant contains almost all of the ruthenium added to the solution. The monomer and the $RuCl_3$ do not significantly bind to the nanotubes.

We believe that the ruthenium decamer is strongly bound to the CNTs. Therefore, once all of the high valence cation is bound to the CNTs, it no longer acts to coagulate the remainder of the suspension, as illustrated in Figure 2B. This claim is supported with SEM and AFM data below and by attempts to extract the decamer from the nanotubes.

Representative FE-SEM images of CNTs deposited from DMF onto an oxide-coated Si substrate are shown in Figure 3. Pristine CNT bundles are imaged easily as shown in Figure 3A. The purity of the samples is high with an occasional contaminant found. CNTs shown in Figure 3B were coagulated from the addition of ruthenium monomer at a concentration of 6 μM. After brief sonication, 10 μL of the unstable dispersion was dropped onto the substrate. We observed a slightly higher density of particles within the deposition. However, images such as that of Figure 3B are not significantly different than those from the pristine tubes. The inset of Figure 3B shows one of the particles at 8X higher magnification. These few particles are similar in morphology to precipitates of the ruthenium salt adhered to the top of the nanotube mat and elsewhere throughout the substrate. FE-SEM images such as that shown in Figure 3C are markedly different to those of parts A and B of Figure 3. CNTs shown in Figure 3C were coagulated from the addition of ruthenium decamer at a concentration of 0.8 μM and treated in a similar fashion. Even though the decamer concentration was ~10X lower than the monomer's concentration, the density of particles atop the nanotube mat is far greater. Many of these

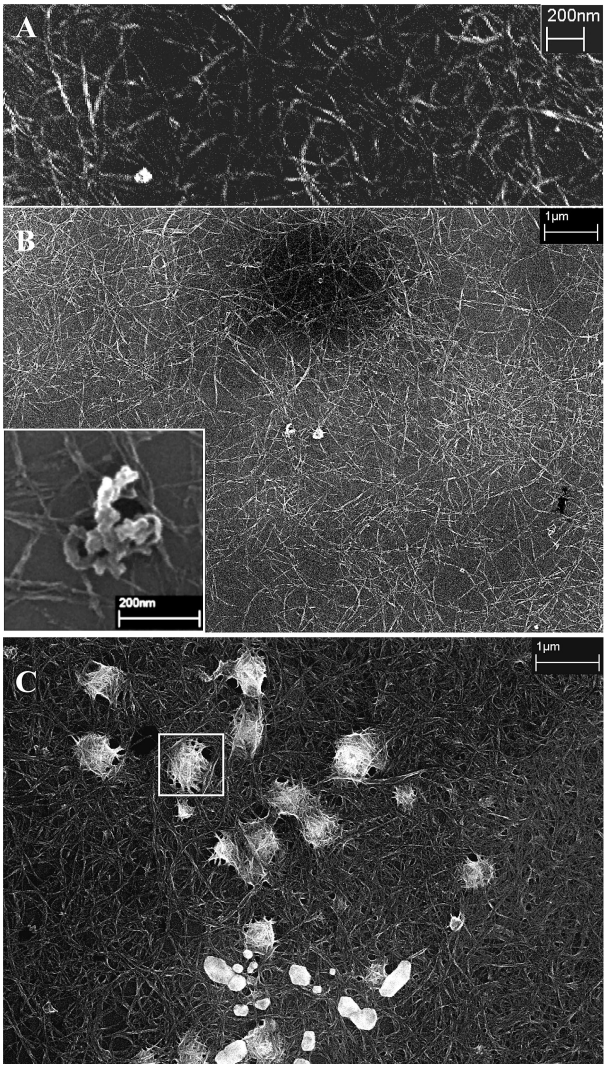

Figure 3. FE-SEM Images (10 kV) of CNTs deposited from DMF on an oxide-coated Si wafer, scale bars indicated for each. Nanotube bundles from pristine untreated CNTs are found to be highly pure as shown in the representative image of (A). Images (B) monomer at 6×10^{-6} M and (C) decamer at 8×10^{-7} M are deposited after coagulation with ruthenium complex. The inset in (B) was acquired at higher magnification to detail the adsorbed particle shown which differs in morphology from those found in the decamer-coagulated mats.

particles are apparently similar to precipitates of the ruthenium salt. There are many regions throughout these micrographs that indicate strong interaction between the decamer and the nanotubes. One of these regions is highlighted by the white box in Figure 3C. Nanotubes appear to be interconnected by the decamer, a CNT−decamer assembly. CNT composites of Ru(diimine)$_3$-poly(4-vinyl)pyridine metallopolymer have been reported.[37] Pyridine and other imines are known to associate with CNTs, which results in the wetting of these polymers to the nanotubes resulting in the thick polymer films observed. Metallodendrimers in this study differ significantly from these polymers in that the decamer we are using is molecularly rigid and the imine functionality is coordinated to the metal center and not easily accessible as an exoreceptor. The imine functionality on the phenazine bridges can coordinate as an exo- or endoreceptor at the "three-centered" or "five-centered" sites, respectively, as described above. Stoddart et al. found that highly charged supramolecular coordination polymers wrapping around SWNTs[38] increased the CNT solubility in MeCN/H_2O solution. This result is not consistent with our coagulation results or with

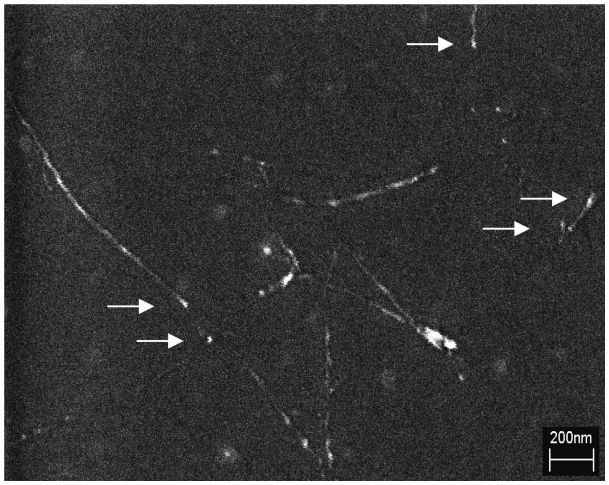

Figure 4. FE-SEM at low accelerating voltage (2 kV) enables imaging of nanotubes on the surface away from the CNT mat. These CNTs were coagulated with ruthenium decamer, and the flocs were collected by centrifugation. The flocs were then extracted with MeCN to remove and unbound ruthenium decamer. The flocs were again collected and redispersed into DMF and deposited on an oxide-coated Si wafer. Bright ends of many tubes are highlighted by arrows. Lateral dimensions are broadened due to electrostatic effects at the surface.

the expectation that high ionic strength solutions tend to coagulate CNTs. Their observation of increased solubility in a mostly aqueous solution indicates significant binding and/or wrapping around the nanotubes, typical of other noncovalent surfactant solubilization.[39] Infrequently, we observe decoration along the length of the tube in our AFM data. Predominantly, we observe specific binding of the decamer at the tube's ends, as discussed below.

Ru binding to the CNT flocs has been confirmed by AA as described above. Decamer-coagulated and MeCN-extracted flocs were deposited and examined by EDX. The ruthenium signal was measured throughout the CNT mats (EDX detection limits are ~1000 ppm). SEM images of the CNT−decamer sample in Figure 3 are consistent with the ccc results above and the multiple binding sites on the decamer itself. While the actual binding model is not determined, vdW $\pi-\pi$ stacking interactions and columbic attraction between the decamer and carboxylate groups on the CNTs are likely dominant.

FE-SEM images at low electronvolts have been shown to accentuate isolated CNTs adsorbed to surfaces through charge contrast imaging.[40−42] We have imaged isolated nanotubes from 3 keV down to 0.4 keV. The FE-SEM image in Figure 4. was acquired at 2 keV. Isolated nanotubes are found sporadically across the surface far from deposition of the nanotube mats. Nanotubes in this image were first coagulated from a stable DMF dispersion by addition of ruthenium decamer. Flocs were separated by centrifugation and extracted with MeCN to remove unbound decamer. At low electronvolts, the nanotubes appear decorated. Interestingly, the ends of many of these CNTs are bright as indicated by the arrows in the figure. While the contrast mechanism of low electronvolt SEM is not clear, the scattering at the ends of these tubes appears different.

AFM images of deposited CNTs treated with decamer look very similar to the FE-SEM data, as illustrated in Figure 5. Because of AFM tip convolution effects, the lateral resolution of the decamer interacting with the nanotubes is poor when scanning over a loosely packed CNT mat. The AFM image in Figure 5 was from deposited CNTs that were coagulated with decamer, then extracted with MeCN, redispersed, and dropped onto the substrate. The deposited sample was treated with

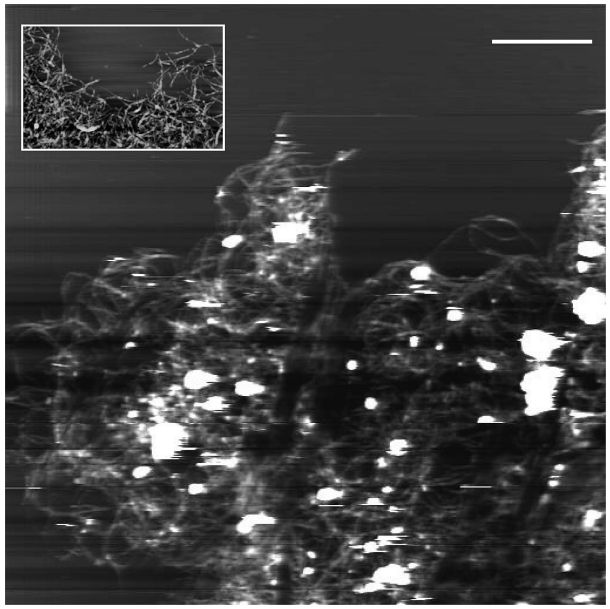

Figure 5. AFM image of CNTs deposited from an extraction of decamer-induced coagulation. Flocs were redispersed in MeCN to extract any residual decamer. Similar extraction of monomer coagulants removed all of the ruthenium, and no particles are found. An AFM of pristine CNT mat is shown in the inset. Scale bar is 5μm.

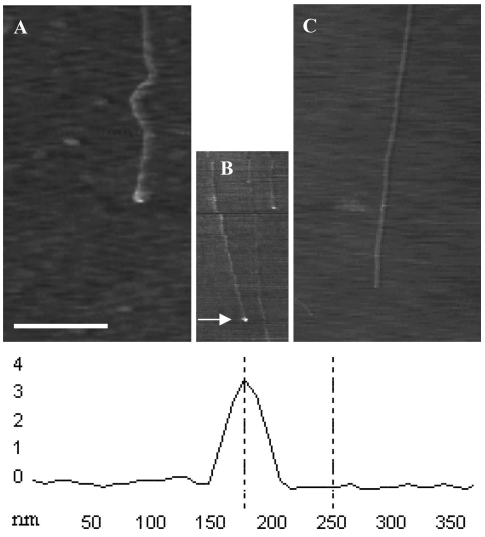

Figure 6. Representative AFM images of isolated CNTs deposited onto oxide-coated Si wafers. The scale bar for (A−C) is 1 μm. All of the CNTs are about 1 nm high. The two CNTs in (C) were deposited from a DMF solution of pristine/unmodified nanotubes. The AFMs of pristine nanotubes do not exhibit decoration along their length or at their ends. Images (A− and B) are from decamer-coagulated CNTs. Flocs of nanotubes were redispersed in MeCN to remove any loosely bound ruthenium complex. Nanotubes were then redispersed in DMF and deposited onto an oxide-coated Si wafer. The line scan shown at the bottom of the figure was across the decamer bound to the CNT end in (B) indicated by the arrow. The width of the trace is convoluted by the AFM probe tip diameter. These data are consistent with our proposed model of site-specific binding to the CNTs.

MeCN. The bright spots atop the nanotube mat do not easily wash away. There are no particles or bright spots found away from the nanotube mats except when associated with a CNT end. The inset of Figure 5 is of a CNT mat deposited from pristine nanotubes (no ruthenium). We do not observe these bright spots on the mats of pristine CNTs.

When AFM images are taken far away (~100 μm) from the "bulk" deposition areas, we find aligned, individual SWNTs interacting with ruthenium decamer complexes. These nanotubes vary in diameter (by AFM height measurement) from 0.6 to 2.3 nm (1.5 ± 0.7 nm for all CNTs diameters measured ±95% confidence interval). Most CNTs are 1−10 μm in length. These dimensions are consistent with HiPco tubes imaged by AFM.[43] AFM of isolated pristine SWNTs is straightforward. The AFM data in Figure 6C shows a representative image of a pristine SWNT which looks similar to many other images of isolated pristine CNTs. AFM images in parts A and B of Figure 6 are of CNTs that have been coagulated by decamer and extracted with MeCN and deposited onto an oxide-coated Si substrate. These nanotubes have a height of ~0.9 nm. At the end of all of the nanotubes is a bright spot. We do not find this on pristine nanotubes or on nanotubes coagulated from Ru monomer. The line scan across one of these bright spots (indicated by the arrow) is shown at the bottom of the image. The height of the cross-section is consistent with decamer bound to the end of the tube. We have reproduced these results many times. For decamer-coagulated nanotubes, nearly all of the CNT ends are associated with a bright spot. We infer that these bright spots are ruthenium decamer in some arrangement strongly associated with the CNT.

Figure 7 is a compilation of several representative AFM images illustrating the binding of ruthenium decamer to isolated SWNTs. In general, the decamer is strongly bound to the end of the nanotube. Most of our AFM data only images one end of the CNT at a time. Although rare, we do observe the decamer attached to both ends of the same tube as shown in Figure 7C (annotated with arrows). There are several instances where we observed decamer bound along the CNT's length. The square highlight in Figure 7A annotates an example of a decamer bound to the midsection of a CNT as it crosses over another CNT. Another decamer that appears to be bound to a midsection of a SWNT in Figure 7A (annotated with arrows and difficult to see in print) is actually at the termini of a second SWNT that is meandering very close to the nanotube just mentioned above. For clarity, we have placed an arrow indicating the decamer-bound CNT end in the AFM images.

When we deposit a coagulated ruthenium complex−CNT solution, we always observed small precipitate particles throughout the surface. These precipitate particles are easily removed by extraction of the flocs with MeCN. When we coagulate the CNTs with ruthenium monomer or 10^{-6} M $RuCl_3$, we observe particles with heights of 2.1 ± 1 nm and 11.6 ± 3 nm, respectively. These particles are never specifically associated with the CNTs. When those samples are extracted with MeCN, we do not observe the particles. Decamer particles that are unassociated with a CNT have a height of 5.5 ± 2 nm. All unassociated particles are easily removed by extraction with MeCN.

When excess decamer is extracted from the coagulant, followed by deposition of the redispersed CNTs, we always observed nearly clean surfaces and SWNTs terminated at their ends by decamer. We never observe these features in our control experiments on pristine CNTs or those tubes extracted from coagulation with ruthenium monomer or $RuCl_3$.

There is a distribution of heights at the ends of the decamer-terminated CNTs. Differences in height are measured by taking a cross-section parallel to the AFM scan direction and along the parallel of the CNT axis. Both cross-sections are through the apex of the bright spot. On average, these "decamer−CNT" termini are 5.0 ± 2 nm high from the substrate. These heights are consistent with our binding model.

From the UV−Vis and AA spectroscopy discussed above, we have calculated the loading of decamer onto the CNTs. With

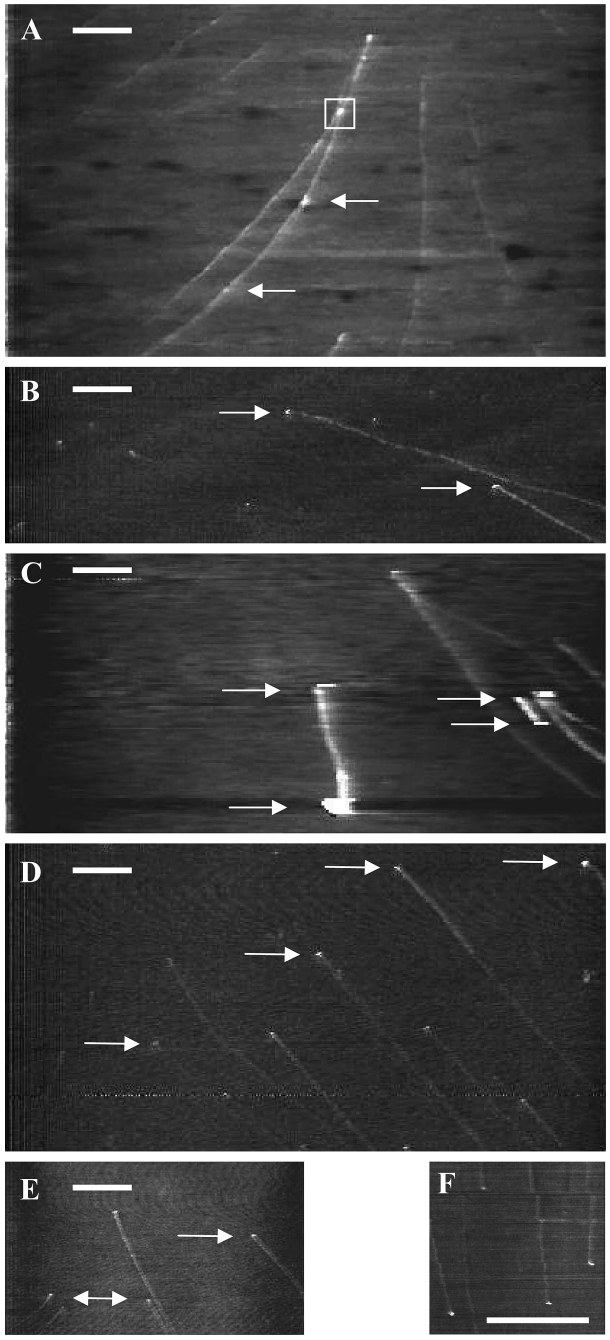

Figure 7. Representative AFM images of decamer-coagulated CNTs. Flocs of nanotubes were redispersed in MeCN to remove any loosely bound ruthenium complex. Nanotubes were then redispersed in DMF and deposited onto oxide-coated Si wafer. The scale bar is 1 μm for parts A−F.

20 ng of decamer added (3×10^{-12} mol), 4.8 μg of CNTs coagulated from solution, 4100 ppm loading, while 200 ng of decamer coagulated 9.0 μg of CNTs from solution, resulting in a 22 000 ppm loading. We are not able to detect any Ru in the remaining stable CNT dispersion, but we assume there must be some decamer bound to any nanotubes still in solution. As shown in Figure 2C, 21 μg of dispersed CNTs was completely coagulated by the addition of 2 μg of decamer (95 000 ppm loading) with no detectable ruthenium left in the clear and colorless solution. In contrast, after coagulation of nanotubes with ruthenium monomer, nearly all of the added Ru remains in solution. Ruthenium monomer and the $RuCl_3$ seem to behave as simple charged coagulants. The behavior of the decamer with the nanotubes is more involved.

IV. Conclusions

Using solution phase spectroscopy, SEM, and AFM results, we have shown specific binding of the supramolecular ruthenium decamer complex to dispersed SWNTs. The decamer binds strongly to the nanotubes under conditions where the ruthenium monomer and other ruthenium salts are easily washed away. Moreover, decamer binding to the ends of the CNTs suggests a specific binding mechanism. Further studies will include high-resolution techniques like transmission electron microscopy and low-temperature, ultrahigh-vacuum, scanning tunneling microscopy and tunneling spectroscopy. These higher resolution methods will help elucidate the nature of this assembly process. We postulate that the observed heights of decamer bound to CNT ends, 5.0 ± 2 nm, supports our binding model of Figure 1 which predicts a particle height of $\sim$5.9 nm. Variations in tilt angle due to coupling to CNTs of different diameters can rationalize our observed variations in "decamer−CNT" height. It is likely that columbic attraction between the decamer and carboxylate anions common to the ends of CNTs direct the binding mechanism. Our observation that the ruthenium monomer does not bind to the ends of the CNTs implies a more involved attachment scheme for the decamer. Enhanced loading of decamer onto the nanotubes at higher decamer concentrations is not consistent with the Schulze−Hardy rule and needs further investigation. These first results do indicate that self-assembled nanostructures made of interconnected CNTs may be facilitated using this class of rigid supramolecular metallodendrimers.

Acknowledgment. We are deeply indebted to Professor F. M. MacDonnell at the University of Texas at Arlington for his generous donation of the ruthenium metallodendrimer $[\Lambda_6\Delta_3\Lambda\text{-}Ru_{10}]^{20+}[PF_6^-]_{20}$. This research was supported in part by an award from Research Corporation and from the NSF (Grant No. 0404193). We also thank Dr. Cliff Carlin for his help with the AA and Dr. Jon Merkert for his help and expertise on the properties of the ruthenium complexes.

References and Notes

(1) Jiang, K. L.; Li, Q. Q.; Fan, S. S. *Nature (London)* **2002**, *419*, 801.
(2) Tans, S. J.; Verschueren, A. R. M.; Dekker, C. *Nature (London)* **1998**, *393*, 49.
(3) Avouris, P.; Appenzeller, J.; Martel, R.; Wind, S. J. *Proc. IEEE* **2003**, *91*, 1772.
(4) Avouris, P. *MRS Bull.* **2004**, *29*, 403.
(5) Misewich, J. A.; Martel, R.; Avouris, P.; Tsang, J. C.; Heinze, S.; Tersoff, J. *Science* **2003**, *300*, 783.
(6) Zhu, J.; Yudasaka, M.; Zhang, M. F.; Iijima, S. *J. Phys. Chem. B* **2004**, *108*, 11317.
(7) Nakashima, N.; Tomonari, Y.; Murakami, H. *Chem. Lett.* **2002**, *6*, 638.
(8) Stevens, J. L.; Huang, A. Y.; Peng, H. Q.; Chiang, L. W.; Khabashesku, V. N.; Margrave, J. L. *Nano Lett.* **2003**, *3*, 331.
(9) Carrillo, A.; Swartz, J. A.; Gamba, J. M.; Kane, R. S.; Chakrapani, N.; Wei, B. Q.; Ajayan, P. M. *Nano Lett.* **2003**, *3*, 1437.
(10) Zheng, M.; Jagota, A.; Semke, E. D.; Diner, B. A.; McLean, R. S.; Lustig, S. R.; Richardson, R. E.; Tassi, N. G. *Nat. Mater.* **2003**, *2*, 338.
(11) Nepal, D.; Sohn, J. I.; Aicher, W. K.; Lee, S.; Geckeler, K. E. *Biomacromolecules* **2005**, *6*, 2919.
(12) Ellis, A. V.; Vjayamohanan, K.; Goswaimi, R.; Chakrapani, N.; Ramanathan, L. S.; Ajayan, P. M.; Ramanath, G. *Nano Lett.* **2003**, *3*, 279.
(13) Richard, C.; Balavoine, F.; Schultz, P.; Ebbesen, T. W.; Mioskowski, C. *Science* **2003**, *300*, 775.
(14) Chen, J.; Liu, H. Y.; Weimer, W. A.; Halls, M. D.; Waldeck, D. H.; Walker, G. C. *J. Am. Chem. Soc.* **2002**, *124*, 9034.
(15) Guldi, D. M.; Rahman, G. M. A.; Jux, N.; Balbinot, D.; Hartnagel, U.; Tagmatarchis, N.; Prato, M. *J. Am. Chem. Soc.* **2005**, *127*, 9830.
(16) Tagmatarchis, N.; Prato, M. *J. Mater. Chem.* **2004**, *14*, 437.
(17) Frehill, F.; Vos, J. G.; Benrezzak, S.; Koós, A. A.; Kónya, Z.; Rüther, M. G.; Blau, W. J.; Fonseca, A.; Nagy, J. B.; Biró, L. P.; Minett, A. I.; in het Panhuis, M. *J. Am. Chem. Soc.* **2002**, *124*, 13694.

(18) Osswald, F.; Vogel, E.; Safarowsky, O.; Schwanke, F.; Vogtle, F. *Adv. Synth. Catal.* **2001**, *343*, 303.
(19) Elizarov, A. M.; Chiu, S.-H.; Glink, P. T.; Stoddart, J. F. *Org. Lett.* **2002**, *4*, 679.
(20) Wildoer, J. W. G.; Venema, L. C.; Rinzler, A.; Smalley, R.; Dekker, C. *Nature (London)* **1998**, *391*, 59.
(21) Kim, M. J.; MacDonnell, F. M.; Gimon-Kinsel, M. E.; Du Bois, T.; Asgharian, N.; Griener, J. C. *Angew. Chem., Int. Ed.* **2000**, *39*, 615.
(22) MacDonnell, F. M.; Bodige, S. *Inorg. Chem.* **1996**, *35*, 5758.
(23) Bodige, S.; Torres, A. S.; Maloney, D. J.; Tate, D.; Kinsel, G. R.; Walker, A. K.; MacDonnell, F. M. *J. Am. Chem. Soc.* **1997**, *119*, 10364.
(24) MacDonnell, F. M.; Ali, M. D. M.; Kim, M. J. *Comm. Inorg. Chem.* **2000**, *22*, 203.
(25) Lehn, J.-M. *Supramolecular Chemistry Concepts and Perspectives*; VCH: Weinheim, Germany, 1995.
(26) Leung, K. C.-F.; Arico, F.; Cantrill, S. J.; Stoddart, J. F. *J. Am. Chem. Soc.* **2005**, *127*, 5808.
(27) Ali, M.; MacDonnell, F. M. *J. Am. Chem. Soc.* **2003**, *125*, 2014.
(28) Paloniemi, H.; Aaritalo, T.; Laiho, T.; Liuke, H.; Kocharova, N.; Haapakka, K.; Terzi, F.; Seeber, R.; Lukkari, J. *J. Phys. Chem. B* **2005**, *109*, 8634.
(29) Bahr, J. L.; Mickelson, E. T.; Bronikowski, M. J.; Smalley, R. E.; Tour, J. M. *Chem. Commun.* **2001**, 193.
(30) Gerdes, S.; Ondarcuhu, T.; Cholet, S.; Joachim, C. *Europhys. Lett.* **1999**, *48*, 292.
(31) Fu, K. F.; Sun, Y. P. *J. Nanosci. Nanotechnol.* **2003**, *3*, 351.
(32) Sano, M.; Okamura, J.; Shinkai, S. *Langmuir* **2001**, *17*, 7172.
(33) Israelachvili, J. *Intermolecular and Surface Forces*, 2nd ed.; Academic Press: London, 1992.
(34) Hardy, W. B. *Proc. R. Soc. London* **1900**, *66*, 110.
(35) Overbeek, J. T. G. *Pure Appl. Chem.* **1980**, *52*, 1151.
(36) Overbeek, J. T. G. *Adv. Colloid Interface Sci.* **1982**, *16*, 17.
(37) Frehill, F.; inhet Panhuis, M.; Young, N. A.; Henry, W.; Hjelm, J.; Vos, J. G. *J. Phys. Chem. B* **2005**, *109*, 13205.
(38) Chichak, K. S.; Star, A.; Altoé, M. V. P.; Stoddart, J. F. *Small* **2005**, *1*, 452.
(39) Hu, C. G.; Chen, Z. L.; Shen, A. G.; Shen, X. C.; Li, H.; Hu, S. S. *Carbon* **2006**, *44*, 428.
(40) Zhang, R. Y.; Wei, Y.; Nagahara, L. A.; Amlani, I.; Tsui, R. K. *Nanotechnology* **2006**, *17*, 272.
(41) Homma, Y.; Suzuki, S.; Kobayashi, Y.; Nagase, M.; Takagi, D. *Appl. Phys. Lett.* **2004**, *84*, 1750.
(42) Croitoru, M. D.; Bertsche, G.; Kern, D. P.; Burkhardt, C.; Bauerdick, S.; Sahakalkan, S.; Roth, S. **2005**, *23*, 2789.
(43) Dyke, C. A.; Tour, J. M. *Nano Lett.* **2003**, *3*, 1215.